Rijksuniversiteit Groningen

Bachelor Thesis

Outgassing and Exoplanet Atmospheres

A study of the effects of outgassing on the temperature and composition of the secondary atmospheres of rocky exoplanets

Author:
R.P. Ferdinand

Supervisor:
F. van der Tak
M. Min

Abstract

This research details the effects of outgassing on the atmospheres of rocky exoplanets. The main focus was to quantify differences in atmospheric temperature as a function of pressure as planetary parameters are varied, as well as studying day-night temperature differences by finding the correlation between night to day flux ratio and pressure, and by determining whether these differences can be observed by JWST.

Temperature profiles were generated in a program called ARCiS, using the planet TRAPPIST-1b as a base model, to study changes in temperature behavior for four generic types of planetary crust: Continental Crust, Bulk Silicate Earth, MORB and CI-Chondrite. Furthermore, four planetary parameters (mass, albedo, radius and orbital radius) were varied to observe changes with respect to this base model. Increasing planet radius, mass and albedo yielded no significant change with respect to the base model. However, an increase of the orbital radius causes a gradual temperature shift between BSE-atmospheres and CC-atmospheres. It was also found that ARCiS does not seem to generate accurate temperature profiles for atmospheres which are too transparent for thermal emissions.

For the day-night temperature differences, a python script was written which allows one to calculate the night to day flux ratio for any tidally locked rocky exoplanet orbiting an ultracool star. Emission spectra of the day- and night sides were generated with ARCiS, varying surface pressure and thereby the night to day ratio. These spectra were compared to measurements from Greene et al. (2023) to determine if these flux differences are observable by JWST. The night to day flux ratio seems to increase with surface pressure, but this increase slows down gradually. Parameters such as equilibrium temperature and gravitational acceleration seem to change the overall magnitude of the ratio, but not the shape of the correlation. Furthermore, it was found that JWST should be able to observe these flux differences, as it observes in the right range for both wavelength and flux density.

Contents

1 Introduction

In the field of astronomy, direct observational study of exoplanets is still quite new. Thanks to observation techniques such as spectroscopy, many aspects can be made known, including their composition, mass, size and distance from their host star. Expanding the branch of study of exoplanets is very important, as it allows us to not only learn about these far away worlds, but also about the planets of our own solar system and their evolution. Therefore, it is important to learn as much as possible about these far away worlds.

Currently, more than five thousand exoplanets have been discovered as well as many candidates which are not yet confirmed (Brennan, 2019b). The most common method for discovering exoplanets is called the Transit Method, where a dip in brightness of a star is observed as a planet passes by its host star. currently, over four thousand planets have been discovered in this way and the Transit Method allows one to measure the radius of a planet quite effectively (Brennan, 2019a).

Another common method is called the Radial Velocity Method, where a blue shift/red shift wobble is measured, which is caused by the star moving with a radial velocity due to the planet's gravity. While not as many planets have been discovered using this method as with the Transit Method (approximately 1000 planets (Brennan, 2019a)), it is still widely used. Different characteristics can be seen with this method that cannot be seen with the Transit Method, such as planet mass. Therefore, the two methods are often used in unison.

It is also possible to observe exoplanets through direct imaging. However, this is very difficult to do, as a planet is very dim compared to its star. Still, about seventy planets have been found using this method (Brennan, 2019a).

Another method is typified by using the gravitational lensing effect, which is often used to discover rogue planets, which have no host star and can sometimes cause the light of stars they pass by to bend under their gravity. However, this effect is often very slight and sudden, so it requires observing large portions of the sky for long periods of time. Still, about two hundred planets have been discovered using this method (Brennan, 2019a).

One can also use astrometry, which, like the Radial Velocity Method, involves looking at the radial motion of the star due to the planet's gravity. However, instead of looking at red shift and blue shift wobbles, the change of the star's position relative to other stars is directly observed. This method is very hard to successfully use because these motions are often so small that they are immeasurable. Only two exoplanets have been discovered using this method (Brennan, 2019a).

Exoplanets, just like the planets in our solar system, come in many shapes and forms. There are many possibilities, ranging from rocky planets like Earth, to gas giants much more massive than even Jupiter. Yet even more possibilities lie in the composition and behavior of their atmospheres. Some planets have little to no atmosphere and are considered bare rocks. An example of this type in our own solar system is the planet Mercury, which receives a large amount of sunlight on its day side, warming it up intensely to about 700 K. However, its night side receives no solar radiation, and due to there being little to no atmosphere, heat is not transferred to the night side through atmospheric convection, and thus, temperatures on the night side can get as low as 100 K.

The opposite is true on a planet with a thick atmosphere, such as Venus. Through convection, heat is transferred from the day side to the night side. On Venus, which is a very extreme example, this convection is very effective due to the atmospheric thickness. This causes there to be very little difference between the day- and night sides.

In planetary science, two types of atmospheres are distinguished: primary atmospheres and secondary atmospheres (Kite and Barnett, 2020). A primary atmosphere is directly formed from

the stellar disk in which the planet and the host star were formed. They therefore contain mostly hydrogen and helium. Gas giants such as Jupiter and Saturn are prime examples of planets that still retain their primary atmospheres.

Many planets either lose their primary atmospheres due to radiation from the star or they never accumulate a significant amount of primordial gas in the first place. Some of these planets remain bare and never gain a significant atmosphere. However, other planets form a new atmosphere over time through a process called outgassing, whereby material from a planet's crust is evaporated. These new atmospheres contain mostly heavier molecules, such as CO_2 and H_2O, and are referred to as secondary atmospheres, which are found on rocky exoplanets.

The composition of these secondary atmospheres depends on the materials which have been outgassed from the crust. This composition is expected to have an effect on its temperature structure. For example, an atmosphere containing a large amount of greenhouse gas is expected to trap more heat at the surface, and so it would be expected that the surface temperature is greater than when the same planet has an atmosphere containing a smaller amount of greenhouse gas.

The outgassing process should also depend on factors such as the amount of radiation a planet receives from its star, as different materials have different evaporation temperatures. Another factor that may affect the process is surface gravity. If we have two planets with the exact same atmospheric composition, of which one is of significantly higher gravity, we would expect the higher gravity world to have a more compact and thinner atmosphere, which should be of a lower temperature than that of the lower gravity world, as a thinner atmosphere cools more effectively.

Some more factors that are expected to affect the temperature structure of an atmosphere are albedo and orbital radius. It would be expected that a planet with higher albedo has overall lower temperatures than a planet with lower albedo, as it reflects more light from its star. Similarly, it would be expected that a planet with a large orbital radius to have lower temperatures than a planet with a small orbital radius, assuming of course that the planets both orbit a star with the same mass and temperature.

This leads to our first research question: what does this difference in atmospheric temperature behavior look like? In this research, the atmospheric temperature differences are quantified for rocky exoplanets using a simulation of the outgassing process. Four generic crust types are studied which all have a different composition. Other variables, such as planet mass and planet radius are varied, as these would have an effect on the aforementioned surface gravity. Planetary albedo is also varied, as well as the planet's orbital radius.

We can also expect the temperature structure to differ for different locations on a planet. A factor which plays an important role in this is which side of the planet faces the star. At first glance this may seem obvious, as the night side of a planet should be colder than its day side, but reality is a bit more complicated.

The temperature difference on the day and night sides depends on the planet's atmosphere, and therefore on the outgassing process. It would be expected that a planet with very little atmosphere such as Mercury will not receive any radiation on its night side, while the day side is bombarded with it. We would therefore expect a significant difference between day and night, especially for closely orbiting and tidally locked planets. If a planet is further away from its star, the absolute difference between day and night becomes smaller because the day side becomes colder, but the relative difference between the two sides still remains, as the night side still does not receive any stellar radiation while the day side receives all of it.

In the opposite case, in which there is a very thick atmosphere (such as that of Venus at approximately 100 bar) with a large CO_2 abundance of 99 percent, heat is not only trapped

at the surface but also distributed more evenly throughout the atmosphere through convection, making the relative difference between night and day less significant.

The second research question is thus: what kind of correlation is there between atmospheric surface pressure and these day-night differences? It would be expected that a difference in temperature would translate to a difference in flux. Therefore, a python function was created, which allows one to compute day to night flux ratios for any planet under the assumption that the planet is rocky, tidally locked and orbiting an ultra cool red dwarf star.

Furthermore, these flux differences should be detectable somehow. If we want to learn more about the atmospheric behavior of exoplanets, we need to be able to not only calculate the flux difference, but also observe it. In this research, the focus is placed on observability through the James Webb Space Telescope (JWST), because this telescope is a good option for observing thermal emissions, as it can observe in the infrared, and it encounters no atmospheric interference. Therefore, emission spectra are plotted of the day- and night sides, varying the night to day flux ratio through the surface pressure. These spectra are compared to measurements from literature to see if JWST is able to observe the differences in flux.

2 Theoretical Background

In this section, the theory behind the outgassing process as well as temperature behavior of rocky exoplanets and day-night differences is explored. In order to study differences in the outgassing processes, it is important to introduce which types of crust are distinguished, as well as outline their composition and explain how this would be expected to affect the temperature behavior on rocky exoplanets. For the temperature differences, it is first explored how temperature behaves on rocky exoplanets in general, after which the theory behind calculating the night to day flux ratio is explored.

2.1 Outgassing and Exoplanet Atmosphere Formation

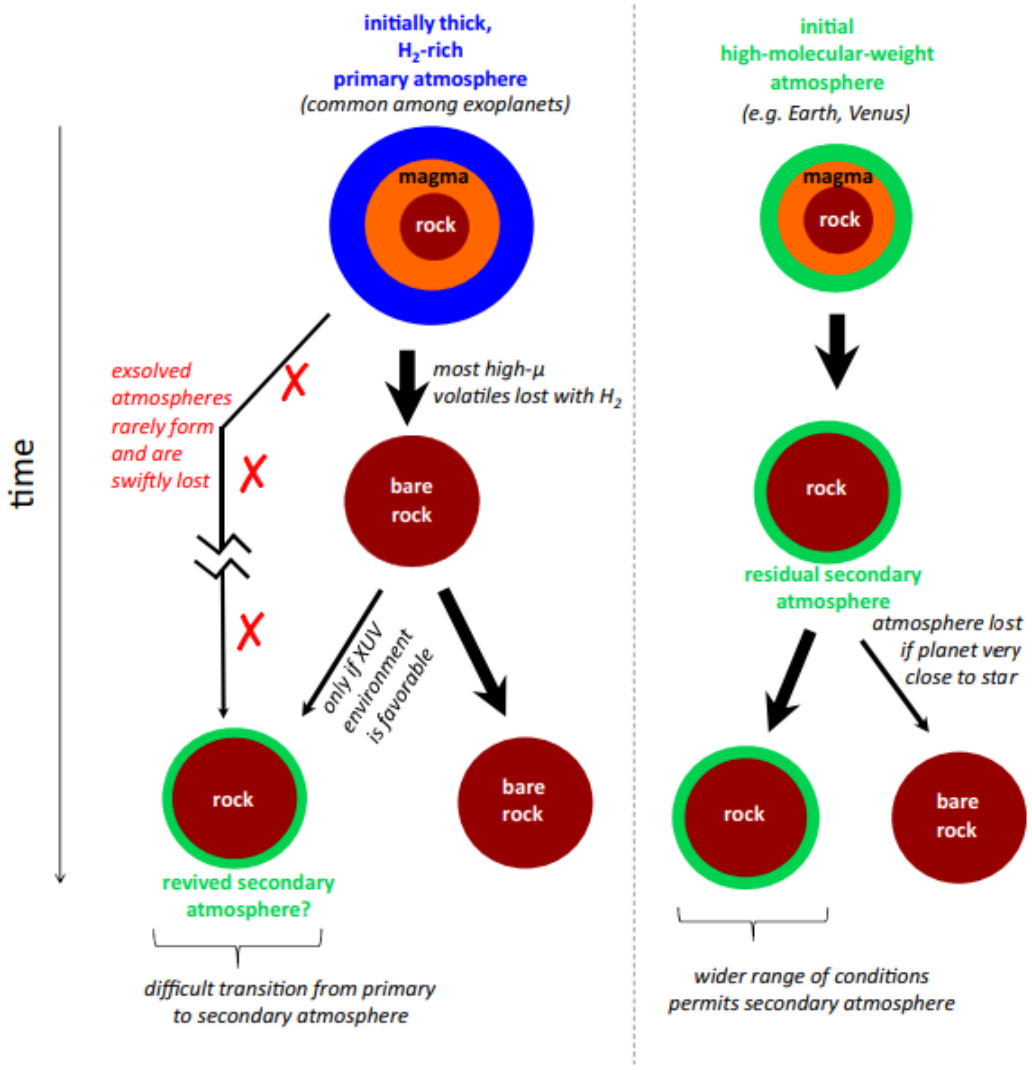

Figure 1: A comparison of the evolution of planets that formed with a H_2 rich primary atmosphere (left), and planets which formed with primary atmospheres containing a higher amount of heavier elements (right). Taken from (Kite and Barnett, 2020). We see that the latter has a higher chance of forming a secondary atmosphere through outgassing.

For young rocky planets that have lost their primary atmospheres, outgassing is believed to be the main process of secondary atmosphere formation (Kite and Barnett, 2020). Due to the internal heat of the young planet, material from the crust is evaporated. This process, over time, forms the planet's secondary atmosphere ((Herbort et al., 2021); (Kite and Barnett, 2020)).

There are many factors that influence the process of secondary atmosphere formation through outgassing. The temperature of and proximity to the host star are both of great importance. The temperature of the host star determines the location of the so-called habitable zone of the system, which depends on the amount of radiation emitted from the host star (Noack et al., 2017). If the planet is too close to the star (beyond the habitable zone) it becomes less likely that the planet retains a thicker atmosphere, because the radiation and stellar winds erode away any atmosphere more quickly (Kite and Barnett, 2020).

The mass of the host star may also play a role. Planets orbiting a lower-mass star (e.g. M-type or K-type) are predicted to have a harder time retaining their atmospheres, because planets orbiting lower mass stars are often bombarded by stellar winds due to their close proximity to their host stars (Kite and Barnett, 2020). Recent JWST observations of the planet TRAPPIST-1b further confirm these expectations. It was found that the planet, which orbits in relative close proximity to its host star, likely has no significant atmosphere (Greene et al., 2023).

Other factors that are more related to conditions on the planet itself include the composition of the crust and of the primary atmosphere the planet initially held ((Herbort et al., 2021); (Kite and Barnett, 2020)). Planets with initially H_2-rich primary atmospheres (such as the very common sub-Neptunes) are less likely to form secondary atmospheres after primary atmosphere loss than planets with primary atmospheres that were more rich in substances with a higher molecular weight (such as CO_2 and water vapor) (Kite and Barnett, 2020) (see Figure 1 for a visual illustration).

The composition of the crust also plays a significant role, which is intuitive because if two planets are completely different in crust composition, one would expect that the outgassing process would result in different atmospheric compositions. Herbort et al. (2021) describes four main categories of crust composition.

Continental Crust (CC) is a felsic composition, meaning that it is rich in silicate compounds such as SiO_2. The reason it is called continental is because on Earth, this type of crust results from plate tectonics. From Table 2 in Appendix B, we see that it is most abundant in oxygen (47%) and silicon (29%), but it also contains a fair amount of aluminum (8%) and iron (4%).

Bulk Silicate Earth (BSE) is an approximation of the materials of which the Earth is composed down to the core (not including the core itself). This would result in a crust composition relatively rich in sillicates containing FeO (rust) and MgO, but relatively poor in elements such as carbon or nitrogen. Like Continental Crust, BSE is slightly less abundant in oxygen (44%) and silicon (21%) and calcium (2.5%). Unlike CC, BSE contains a significant amount of magnesium (about 22%, compared to 2.2% for CC (Herbort et al., 2021)).

Mid Oceanic Ridge Basalt (MORB) is a composition which on Earth is found at the bottom of the oceans. As the name suggests, this composition is relatively rich in basalt, which is a type of mafic rock (e.g. rich in magnesium and iron) (Herbort et al., 2021). From Table 2 in Appendix B we see that this crust type mostly contains oxygen (44.5%), silicon (24%), calcium (8%) and aluminum (8%) and it does indeed contain a fair amount of magnesium (5%) and iron (7%) as well.

CI-Chondrite is a particularly interesting type of crust, as it is believed to be the remainder of the formation period of the planet. It is very abundant in oxygen (46%), iron (19%) and silicon (11%), and also contains a fair amount of sulphur (5.5%). It is the most abundant in carbon out

of all four crust types at 3.5%. It is a type of crust which on Earth would result from meteorite impacts and it is very useful for studying the early stages of a planet's formation.

A planet's total outgassing is very much dependent on the composition of the crust, as well as on the aforementioned factors. The total outgassing is determined by which crust elements are evaporated and by the quantity in which this occurs. It would be expected that atmospheres outgassed through CC have a different composition than those outgassed through BSE, MORB and CI-Chondrite. Therefore, atmospheres which are outgassed through different crust compositions should behave differently in their temperature structures.

If we look at Table 2 in Appendix B, we see that BSE is relatively poor in carbon and hydrogen compared to the other crust types. The opposite is true for CI-Chondrite, which is relatively rich in carbon and hydrogen. This means that we would expect BSE to outgas the least CO_2 and methane, and CI-Chondrite the most. This difference between greenhouse gas abundances should cause significant differences in resulting temperature profiles.

There are of course, still other factors, such as planet mass and density. The presence of a magnetic field would also have an important influence on the formation of an atmosphere, as it would shield the planet from stellar winds, allowing it to retain a thicker atmosphere. However, for the purpose of this research, magnetic effects are neglected.

2.2 Exoplanet Temperatures

The temperature on the surface of a planet depends on many different factors. We can compute its so-called equilibrium temperature, which is the temperature a planet would have if it were in thermal equilibrium with its surroundings, and is usually given by (Del Genio et al. (2019); Pater and Lissauer (2015)):

$$T_{eq} = \left(\frac{S_0(1-A)S_{ox}}{4\epsilon\sigma} \right)^{\frac{1}{4}} \tag{1}$$

where S_0 is the Earth's solar constant (which is equal to 1361 W m^{-2} (Del Genio et al., 2019)), A is the planet's bond albedo (or planetary albedo), S_{0x} is the instellation relative to what would be received by Earth, and σ is Stefan-Boltzmann's constant. Instellation is similar to insolation on Earth, except for that it is governed by a different star from our own sun (Del Genio et al., 2019). ϵ is the planet's emissivity, which if we assume the planet radiates as a blackbody, is equal to 1. This is often a good approximation, as its value is usually contained between 0.9 and 1 (Pater and Lissauer, 2015).

The equilibrium temperature is based on many assumptions, mainly the assumption of a planet radiating like a blackbody. This is however, often not the case as planets are often bombarded with radiation and atmospheric convection causes heat to be more evenly distributed. We can expect a planet with an atmosphere that traps a lot of heat through greenhouse gases to have a physical temperature which is higher than the equilibrium temperature. For bare rocks, the night side has a temperature of nearly absolute zero, so the equilibrium temperature is not even close to the planet's physical temperature, which varies greatly throughout the surface.

Other factors, such as planetary albedo, atmospheric composition and position relative to its host star are also very important (Del Genio et al., 2019). While the equilibrium temperature does include some of these parameters, like albedo and orbital radius, atmospheric composition is not taken into account and so it often does not describe the actual conditions on the planet's surface very well. However, the equilibrium temperature is still a very important value as it describes the amount of radiation a planet directly receives from its host star, and is therefore fundamental in studying the thermal processes occurring on rocky exoplanets, even if it is not

its real temperature.

Yet another noteworthy factor is atmospheric optical thickness, which largely governs a planet's heating and cooling rate (Koll, 2022). For a very thick atmosphere rich in greenhouse gases (such as that of Venus which is approximately 92 bar (NASA, 1968)), we would expect a higher overall surface temperature because the greenhouse gases trap heat on the planet's surface, warming it up. On the other hand, a thinner atmosphere would contain a smaller overall amount of gas and in that regard, we would expect it to result in lower surface temperatures (depending on the planet's proximity to its host star). However, a thinner atmosphere would also allow more radiation to hit the surface directly, which warms up the lower atmosphere through heat from the surface itself.

2.3 Day-Night Differences

Temperatures can vary strongly on the side of the planet facing towards its star (the day-side) and on the side facing away from it (the night-side). On the day-side, a planet is being constantly exposed to radiation from its star. On the night side, this is not the case. If we are looking at a bare rock, there is little to no atmospheric convection to transfer heat, and so the night side remains cold, making the difference between day and night very significant.

In the presence of an atmosphere, more heat is retained on the night side. This is because heat is distributed over the planet more evenly through convection processes in the atmosphere, and through winds caused by pressure differences throughout the planet's atmosphere. We would therefore expect the differences between the day- and night-sides to decrease as atmospheric thickness (and thus, surface pressure) is increased.

In the case of a tidally locked planet, where one side is always facing the star, and the other is always facing away from it, it can naturally be expected that differences between day and night temperature are quite extreme. This makes tidally locked exoplanets particularly useful in studying day and night side differences.

One would expect a temperature difference to be translated into a flux difference primarily for infrared thermal emissions. In a research by (Koll, 2022) these flux differences on the day- and night sides of tidally locked rocky exoplanets orbiting ultracool stars were studied. The goal of this research was to develop an analytical model for the heat redistribution of planets of this type which required a derivation of both the day time flux and that of the night time flux.

In the aforementioned research, the flux for the day side was derived (Koll, 2022):

$$F_d = \left(\frac{8}{3} - \frac{5}{3} \frac{\tau_{LW}^{1/3} \left(\frac{p_s}{1bar}\right)^{2/3} \left(\frac{T_{eq}}{600K}\right)^{-4/3}}{k + \tau_{LW}^{1/3} \left(\frac{p_s}{1bar}\right)^{2/3} \left(\frac{T_{eq}}{600K}\right)^{-4/3}} \right) \sigma T_{eq}^4 \tag{2}$$

where k is a packaging value proportional to the gravitational acceleration (Koll, 2022):

$$k \propto g \tag{3}$$

τ_{LW} is the long-wave optical thickness, which says something about how much the material prevents light from passing through it at relatively long wavelengths in the infrared spectrum, p_s is the surface pressure in bar, T_{eq} is the aforementioned equilibrium temperature in Kelvin and σ is Stefan Boltzmann's constant.

For the research conducted in this paper, these equations were very useful in determining the day to night ratio for thermal flux emissions (see Section 3.4). It is however of important note that these equations only work for tidally locked rocky exoplanets orbiting ultracool red dwarfs. therefore, the focus of this part of the research lies there.

Further assumptions include neglecting the planet's internal heating, making the night-side flux equal to the flux at the top of the atmosphere. A one-dimensional atmospheric structure is also assumed. Furthermore, cloud formation and photochemical hazes are not taken into account while deriving these equations (Koll, 2022).

3 Methodology

In this section, the steps which were undertaken in this research are brought into detail. As mentioned earlier, the three main goals of this research were to study changes in the behavior of temperature as a function of pressure in exoplanet atmospheres when certain input parameters are varied (such as planet mass, radius, albedo and distance to the host star), to calculate the ratio of flux between the day and night sides of exoplanets, and to determine whether the difference in temperature between the day and night sides of the planet are observable using JWST.

3.1 An Introduction to ARCiS

ARCiS (short for ARtful modelling Code for exoplanet Science) is a fortran program which simulates the process of outgassing and atmosphere formation, given initial planetary conditions (Min et al., 2020). Using initial input parameters, such as planet mass, radius, distance to its host star, the temperature of its host star and eventual atmospheric pressure, the process of outgassing is simulated, yielding for example temperature profiles, composition plots and spectra of exoplanet atmospheres. In this section, the process through which the program calculates results is explained (see also Figure 2, which illustrates a specific application of the ARCiS program from Min et al. (2020)).

For the setup of the program, several parameters are taken into account. The calculations start from atomic abundances from which the molecules are formed that eventually form the atmosphere. A very important abundance ratio is the C/O ratio, which determines the chemistry of the gas phases (Min et al., 2020).

After the atomic abundances are determined, the next step is taking into account cloud formation (see figure 2). Cloud formation is an important process because it changes the element abundances in the atmosphere (Min et al., 2020). In this research however, cloud formation is not taken into account and the step is replaced by the outgassing process (see Figure 3).

After cloud formation (or in our case, outgassing) is taken into account, the chemistry for the gas phase is determined. The cloud formation takes away some of the element abundances, which means the atmosphere chemistry is variable as a function of position on the planet. Outgassing would instead add to the element abundances. To calculate the chemistry, ARCiS uses another program called GGchem, which is integrated in the code itself (for further reading about GGchem, see Woitke et al. (2018)).

With chemistry calculated, the opacities can be computed. two different opacities are specified: molecular opacity and cloud opacity. The calculations for molecular opacities are made using spectral line-lists for each molecule and their corresponding k-tables (e.g. it does not explicitly calculate the opacities from scratch, but it uses predetermined values from different sources in a database.

For the cloud opacities, some assumptions are made, such as the particles being perfectly spherical in shape. A problem with this assumption is that if the shape of the particles are even slightly different, it will yield completely different results, so therefore a method called the DHS-method is used (short for Distribution of Hollow Spheres). For further reading about this method, see (Min et al., 2005). In our research this is not a problem since cloud formation is not taken into account.

The next step is calculating the temperature structure, which is done with the theory of radiative transfer. As the temperature structures depend heavily on opacity, the calculation needs to be repeated for all the opacities so that we get a full picture (Min et al., 2020).

Another important parameter to be taken into account is scattering. The ARCiS program uses two methods for this. The first method is called Monte Carlo scattering. The scattering

flux is calculated by simulating photon emissions (both from the atmosphere itself and from the host star), and then tracing them through the atmosphere. The other method directly calculates the scattering flux using a matrix inversion (Min et al., 2020).

The final step is calculating the transmission and emission spectra. For the transmission spectra, we want to calculate how much light is blocked by the molecules in the resulting atmosphere. this is done through the opacities mentioned before and by computing the optical depth at varying impact parameters. From this, the effective radius of the planet can also be determined (Min et al., 2020). The emission spectra are calculated using the radiative transfer equation, varying the rays accross the planet.

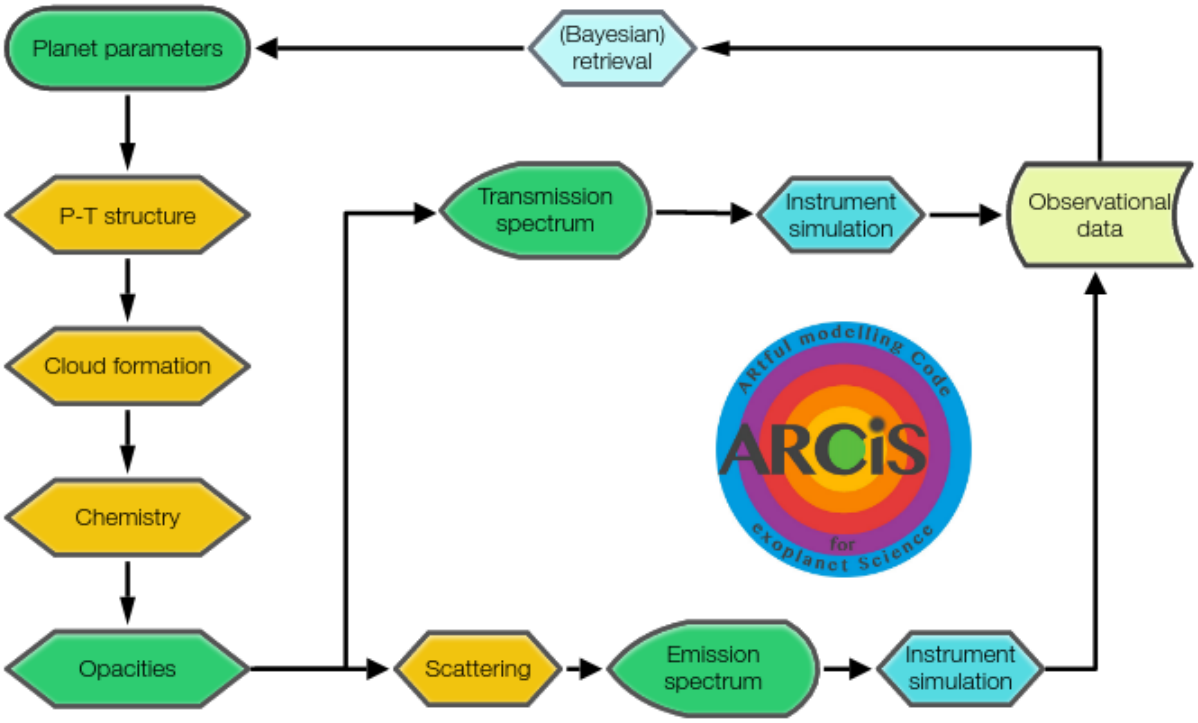

Figure 2: A visual depiction of the order of steps undertaken by ARCiS as the program is run in the specific research of Min et al. (2020).

Another interesting feature of ARCiS is a function that allows for simulations of instrumental observations for which ARCiS uses a retrieval method called 'model constrained retrieval' (Min et al., 2020). In our research however, instrument simulation is not used.

In the research conducted in this paper, ARCiS is used to model the behavior of rocky exoplanet atmospheres under varied conditions of outgassing, as well as modeling differences on the day and night sides of said planets to determine if these differences are visible with JWST (see Figure 3).

3.2 General Steps of Running ARCiS and Analyzing Data

To generate the data used in this research, the ARCiS program requires an input file in which values such as planet mass, radius, the distance of the planet from its host star and its albedo are specified, as well as the resulting surface pressure from the atmosphere (see Appendix C for an example of one such input file). If chosen, certain values can also be taken from an

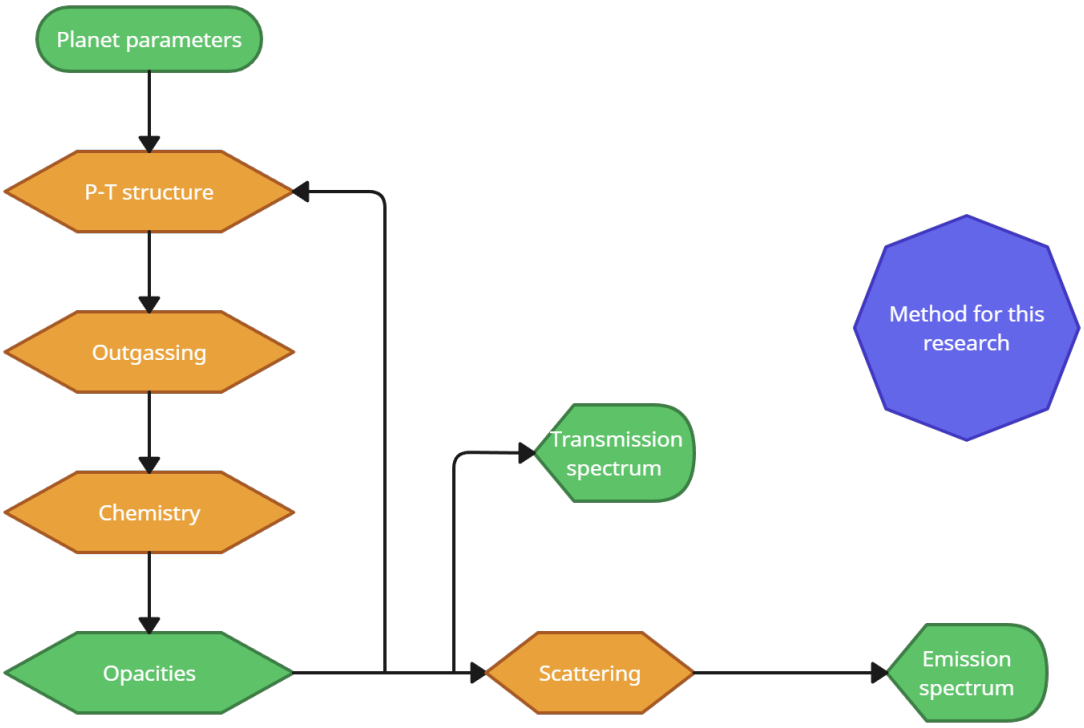

Figure 3: The application of the ARCiS program as it was used for this research. Cloud formation is replaced by outgassing and there are no instrument simulations used. Furthermore, the program iterates over the opacities, first making a guess using the planet parameters, and then narrowing closer to the true value for the opacities, until the difference between iterations becomes negligible or until a maximum number of iterations is reached.

included database of known exoplanets by specifying the planet name. Other properties (such as chemistry) can be calculated while the program is run, or put in manually.

Using this input file, ARCiS generates sets of data. One such data set consists of mixing ratios, which show the abundance of many different elements in the resulting atmosphere as a function of atmospheric temperature and pressure. Emission spectra are also generated, which show the flux (energy per unit area) and corresponding wavelengths. Another important data set is the density profile, which shows values such as temperature, pressure and density as a function of height from the surface.

For the purpose of this research, the main focus was placed on the temperature profiles as a function of pressure, on the emission spectra and on the chemical abundances in the resulting atmosphere. In the first part of this research, input values were varied in order to study changes in behavior of exoplanet atmospheres resulting from changes in the outgassing process. A revised application of the ARCiS program appropriate to this research was used (see Figure 3).

For the day-night differences (see Section 2.3), The ratio of emitted flux between the day and night sides of exoplanets was studied and it was determined whether the difference in flux is visible using JWST, and so the focus was laid on separating the day and night side into two different emission spectra, which could then be compared to literature.

3.3 Studying Atmospheric Behavior by Varying the Outgassing Process

The first step of modeling the behavior of exoplanet temperatures was to create a base model on which all of the simulations thereafter were based. This base model was a rocky exoplanet and the assumption was made of the crust consisting of one of four different crust types, as mentioned earlier: Continental Crust (CC), Bulk Silicate Earth (BSE), Mid-Oceanic Ridge Basalt (MORB) and CI-chondrite (CI). This base model encompassed the temperature profiles of atmospheres resulting from each crust type. The starting values used as input for the ARCiS program were chosen to be based on TRAPPIST-1b.

TRAPPIST-1b is an interesting world in a peculiar solar system. The TRAPPIST-1 system consists of seven planets which are all relatively Earth-like in terms of their mass, size and composition (Gillon et al. (2016); Grimm et al. (2018)), while the solar system itself is relatively small (if placed in our solar system, all of the planets' orbits would fall within the orbit of Mercury (Gillon et al., 2016)). Because the planets of this system are so Earth-like (at least superficially in terms of mass and radius), and because three of the system's planets fall within the star's habitable zone, TRAPPIST-1 is currently widely researched in the search for life on extraterrestrial planets (see for instance Dobos et al. (2019), Grimm et al. (2018) and Brady et al. (2023)), making this planetary system very interesting for the study of exoplanet atmospheres.

While TRAPPIST-1b is much too close to its star to harbor any sort of extraterrestrial life, the planet is still very interesting in the study of atmospheres. It was recently the topic of much debate as apparently no evidence of a significant atmosphere has been found using JWST, while the planet was previously thought to be a Venus-like world with a very dense atmosphere (Crane, 2023). Because of the uncertainty surrounding this situation, TRAPPIST-1b is a very interesting planet to use as a base model. The planet being tidally locked also makes it easier to study temperature behavior. This is why TRAPPIST-1b was chosen for the purpose of this research.

To study the behavior of the temperature profiles, several variables, such as planet mass, radius, albedo and distance from the planet's host star were varied in the ARCiS input file. Changes in the base model were observed for all four crust types. If any significant changes were observed, more data was collected, using smaller variation intervals, to study the evolution of these changes in more detail.

To get a better understanding of this evolution, a closer look was also taken at the chemical abundances in the simulated atmosphere, as well as the infrared emission spectra, to find out which chemicals would be dominant in the atmosphere under specific conditions on the planet, as changes in chemical abundances could correspond to changes in the behavior of the pressure and the temperature. The focus was hereby laid on Continental Crust and Bulk Silicate Earth.

3.4 Day-Night Differences

As was discussed in Section 2.3, a difference in temperature is expected to result in a difference in flux density. Using Equations 2 and 3 (Section 2.3), we write the following equation for the night side flux:

$$F_n = \frac{\frac{1}{k}\left(\frac{p_s^2 \tau_{LW}}{T_{eq}^4}\right)^{1/3} (1bar)^{-2/3}(600K)^{4/3}}{1+\frac{1}{k}\left(\frac{p_s^2 \tau_{LW}}{T_{eq}^4}\right)^{1/3} (1bar)^{-2/3}(600K)^{4/3}} \sigma T_{eq}^4 \tag{4}$$

which is dependent on exactly the same variables as equation 2.

using equation 4 as well as equation 2 for the day-side flux, a python algorithm was written called 'daynight' which calculates the night to day ratio of flux for any tidally locked rocky

exoplanet orbiting a red dwarf star (see Appendix A for the code). The values of k and T_{eq} were given in Koll (2022) for three different planets: TRAPPIST-1b ($k = 1.2$, $T_{eq} = 391$ K), GJ1132b ($k = 1.9$, $T_{eq} = 578$ K) and LHS3844b ($k = 2.3$, $T_{eq} = 805$ K) (see also Table 1 in Appendix B).

These values were used to calculate night to day flux ratios, varying surface pressure from 0.1 bar to 100 bar, in steps of 0.1 bar. Several different scenarios for the long wave optical thickness (τ_{LW}) were also varied, first keeping it fixed at three different values ($\tau_{LW} = 0.1$, $\tau_{LW} = 1$ and $\tau_{LW} = 5$) and then setting it proportional to the surface pressure itself ($\tau_{LW} \propto p_s$), which would be the most realistic scenario, as one would intuitively expect optical thickness to be dependent on atmospheric pressure. For the purpose of this research, a direct linear correlation between p_s and τ_{LW} was assumed, with the proportionality constant set to 1.

The values of the night to day ratio were then plotted against surface pressure for all scenarios of the optical thickness for all three planets. This was done to find a correlation between the night to day ratio and the surface pressure, to see whether or not the correlation is similar for all planets, as well as to observe changes in the correlation through variation of τ_{LW}.

To find out whether the differences in flux could be observable with telescopes such as JWST, literature was consulted which contained information about the pixel sensitivity (e.g. how much flux the telescope can observe and whether the difference would be noticeable) and the range of wavelengths the telescope can observe. Several plots of the emission spectra of TRAPPIST-1b were made to make a comparison between our results and direct measurements of the day side of TRAPPIST-1b by the MIRI element of JWST from Greene et al. (2023).

To generate emission spectra using ARCiS, input values called phases, specifying the planet's position in its orbit were used. Phase 1 was set to be equal to 0°, which would place the planet directly between us and the star. This means that in this phase, the night side is observed. Phase 2 was set to 180° which would place the planet at the opposite side, meaning the day side is observed.

The night to day ratio was calculated for four different values of the surface pressure, namely $P_s = 0.1$ bar, $P_s = 1$ bar, $P_s = 10$ bar and $P_s = 100$ bar. The resulting night to day ratios, as well as the values of the surface pressure itself were put through ARCiS, again setting phase 1 to 0° and phase 2 to 180°. The evolution of the differences on the day and night side was studied and the data was compared to data from literature to determine the visibility through JWST.

4 Results

In this section, the results of the simulations of atmospheric outgassing as well as of the day-night differences are presented. For the ARCiS outgassing simulations, temperature profiles are plotted as a function of pressure as a way to observe differences in temperature and pressure behavior as certain parameters are varied. In Section 4.1, the base model is shown to study the differences in the profiles between the four crust types. In Sections 4.2 and 4.3, parameters are varied to observe deviations from the base model.

In Section 4.4, atmospheric abundance of chemicals (including but not limited to CO_2 and CH_4, which are important greenhouse gases) are plotted against pressure to study the processes behind these deviations. To test these models against observation, emission spectra (flux density versus wavelength) are computed as well.

In Section 4.5 we study the day-night differences. To do this, the night to day flux ratio (F_n/F_d) is plotted against the surface pressure, which was varied between 0.1 bar and 100 bar for the three aforementioned planets (see Section 3.4). Four scenarios for the long wave optical thickness are studied (see sect. 3.3). Finally, in Section 4.6, emission spectra of both the day and night sides of the three planets are plotted to observe the evolution of their differences and to determine whether these differences are observable by JWST.

4.1 The Base Model

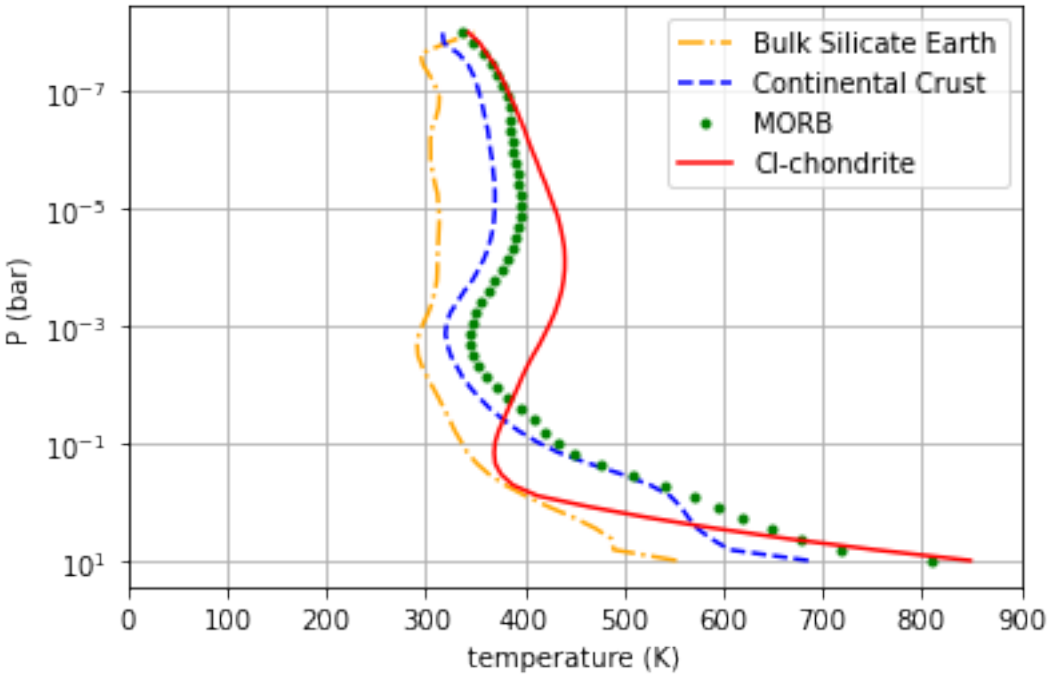

Figure 4: A plot of the base model, where temperature profiles were extracted for atmospheres outgassed through Bulk Silicate Earth, Continental Crust, MORB and CI-Chondrite.

In Figure 4, we plot the temperature as a function of the logarithm of atmospheric pressure for an atmosphere resulting from the simulated outgassing process assuming four different crust types. It is already apparent that they look quite different from one another, especially at higher pressures (e.g. near the planet's surface), where we see significant differences in temperature. The CI-profile seems to deviate the most in shape, seeming to bend for higher pressures.

4.2 The Influence of Planetary Parameters

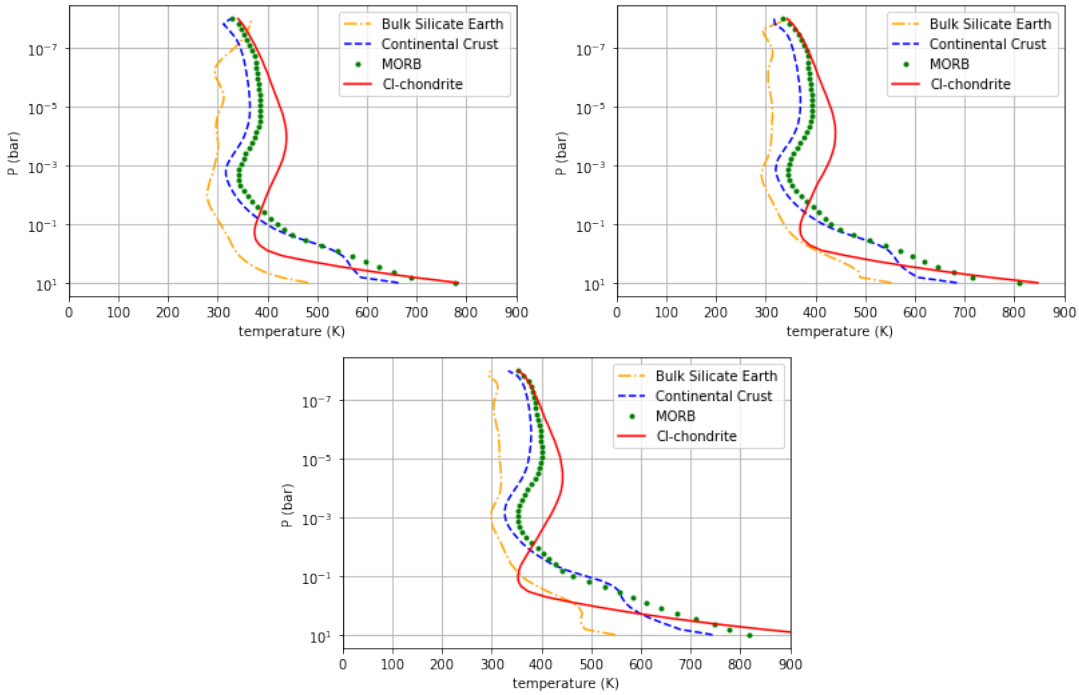

Figure 5: Variations of the base model with increased planet mass (top left), increased albedo (top right), and increased planet radius (bottom). Aside from some slight differences, they all still strongly resemble the base model (see Figure 4).

In Figure 5, we plot deviations of the base model for three varied parameters. In the top left plot, where mass was varied, we see no major difference from the base model. We do observe some slight changes in the temperature at high pressure (e.g. near the surface), especially for atmospheres outgassed through BSE crusts. We see for example that the surface temperature for BSE drops from approximately 550 K (see Figure 4) to slightly below 500 K if planet mass is doubled.

On the top right of Figure 5, the variable that was changed was the planetary albedo, which for the base model is equal to 0.1, but was changed to 0.5. For context: an albedo of zero would mean total absorption of light, and an albedo of one would mean total reflection of all light. The input albedo for ARCiS is wavelength independent. Planet mass has been set back to its base value of 0.0032 M_{jup}. We see that there is little to no deviation from the base model.

For the increase in planet radius (Figure 5, bottom plot), little to no significant changes can be seen from the base model as well, other than some slight increase in temperature for higher pressures for Continental Crust and CI-Chondrite.

4.3 The Influence of the Orbital Radius

In Figure 6, we plot another deviation from the base model, where the distance of the planet from its host star was changed from 0.0115 AU to 0.02 AU. Note that for a small solar system like TRAPPIST-1, this is a significant increase in distance. The planetary radius was set back to its original value of 0.1 R_{jup}.

In Figure 6, we see a lot more deviations from the base model. Firstly, for the base model, we see that temperatures at the planet's surface ($p = 10^1$ bar) are above 500 K for all four crust

types. In the case of an orbit radius of 0.02 AU, the temperature at the surface has decreased to below 500 K for all crust types. Furthermore, we see that a CI-chondrite world still has the highest surface temperature out of all four, sitting just below 500 K, while the other three are sitting around 300 K.

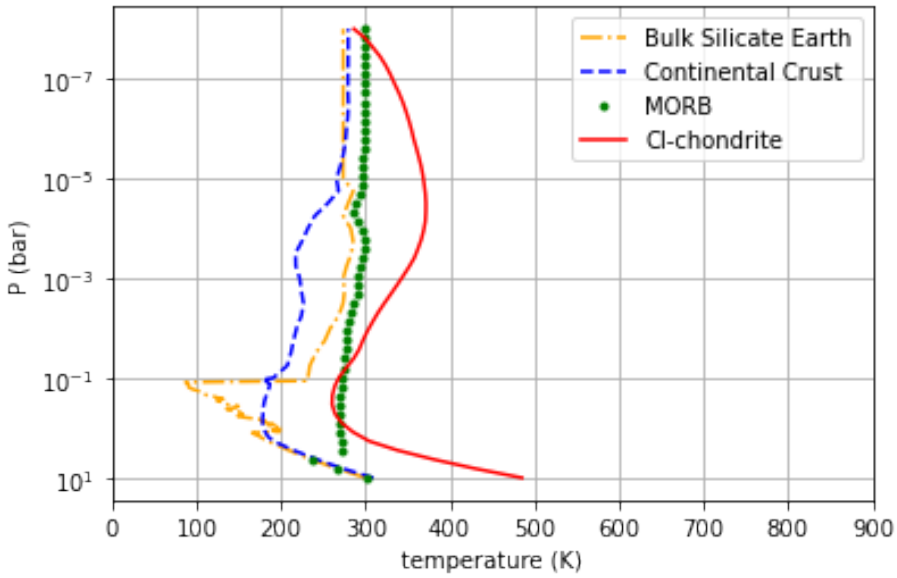

Figure 6: A variation of the base model where the planet's distance from its host star was increased.

,

There also appears to be a shift in temperature order for Bulk Silicate Earth and Continental Crust worlds. In the base model, we see that Continental Crust worlds are for most pressures at a higher temperature than Bulk Silicate Earth worlds, except at the very lowest pressure. In Figure 6, we see that this has shifted significantly, with CC-planets now becoming colder than BSE-planets for higher pressures than before.

For Bulk Silicate Earth, we can also see a very sudden jump in temperature at the 10^{-1} bar mark. The temperature first drops to below 100 K, and then seems to rise very suddenly to 200 K again. Some temperature spikes also seem to appear for Continental Crust and MORB, but are much smaller. In Section 4.2, The focus is put on the temperature shift between Bulk Silicate Earth and Continental Crust. Smaller intervals of orbital distance increase are made to study the temperature shift between CC-atmospheres and BSE-atmospheres in more detail.

In Figure 7, we zoom in on Continental Crust and Bulk Silicate Earth. Smaller intervals of increase are applied for the orbital radius to take a closer look at the observed temperature shift and the sudden temperature drop for BSE-atmospheres. As we can see in the figure, the temperature shift is very gradual as we increase the orbital radius from 0.0115 AU to 0.02 AU. We also see the temperature spike form gradually as distance increases.

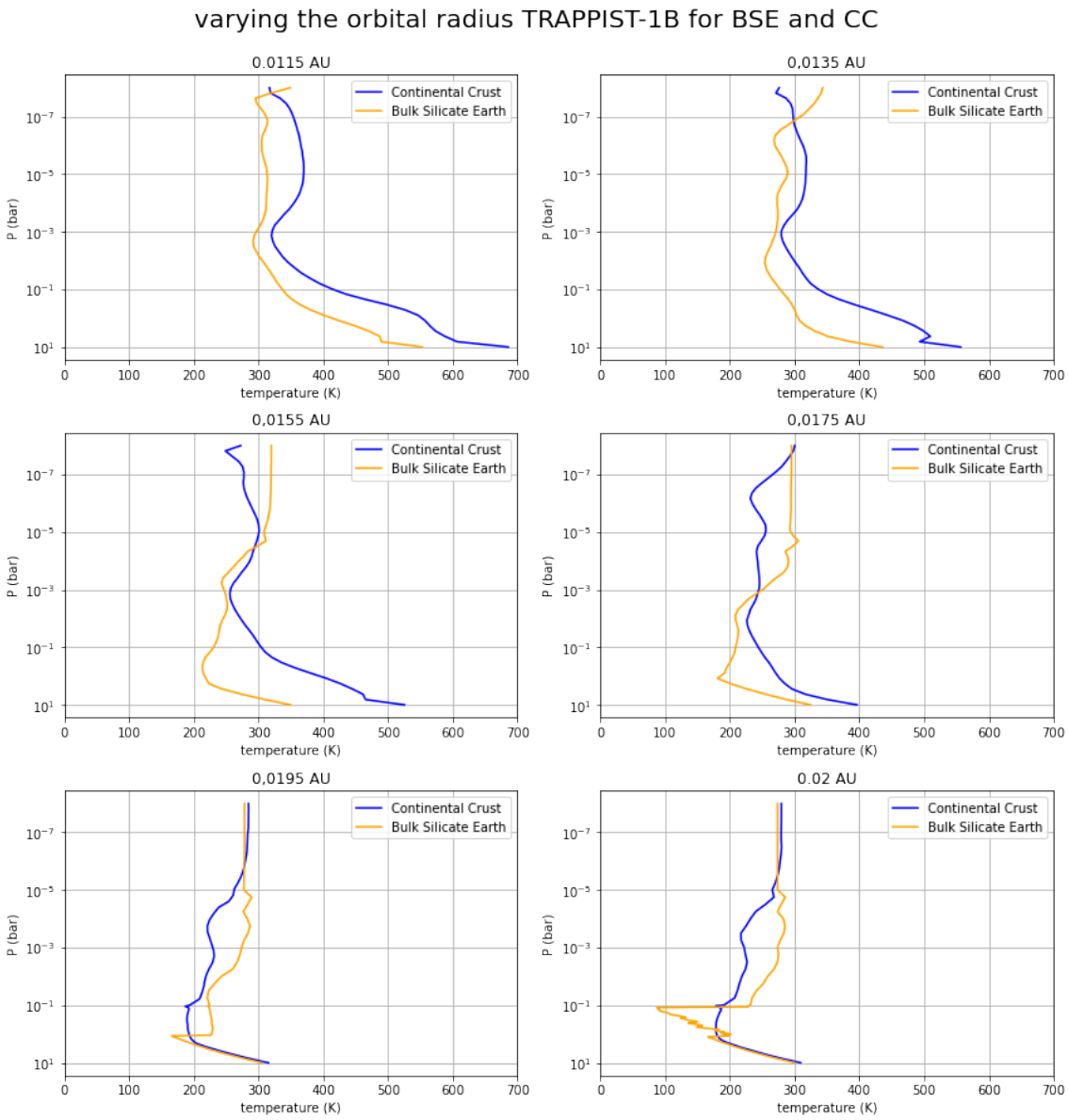

Figure 7: An evolution plot using smaller intervals of increase of orbital radius, focusing on the temperature order switch of the CC-atmosphere and the BSE-atmosphere.

,

4.4 Chemical Abundances and Emission Spectra

The next step was to plot the emission spectra and chemical abundances, which was done in Figures 8 and 9 respectively. As we can see in Figure 8, the emission spectra for the CC-atmosphere looks very similar to the one for the BSE-atmosphere at its initial value of 0.0115 AU, but they become more different as radius is increased.

A smoothening of the emission spectra is also visible, and seems to occur for BSE-atmospheres more quickly than for CC-atmospheres. At the largest distance of 0.02 AU, only the absorption by CO_2 and a bit of H_2O is still visible for both Continental Crust and Bulk Silicate Earth. This indicates that the atmospheres become less and less diverse in its molecular composition. We can also see that BSE-Atmospheres are less abundant in the important greenhouse gas CO_2.

To bring more focus on the abundance of elements which are not visible in the infrared

spectrum (such as nitrogen), Figure 9 shows the abundance of a group of molecules as a function of pressure.

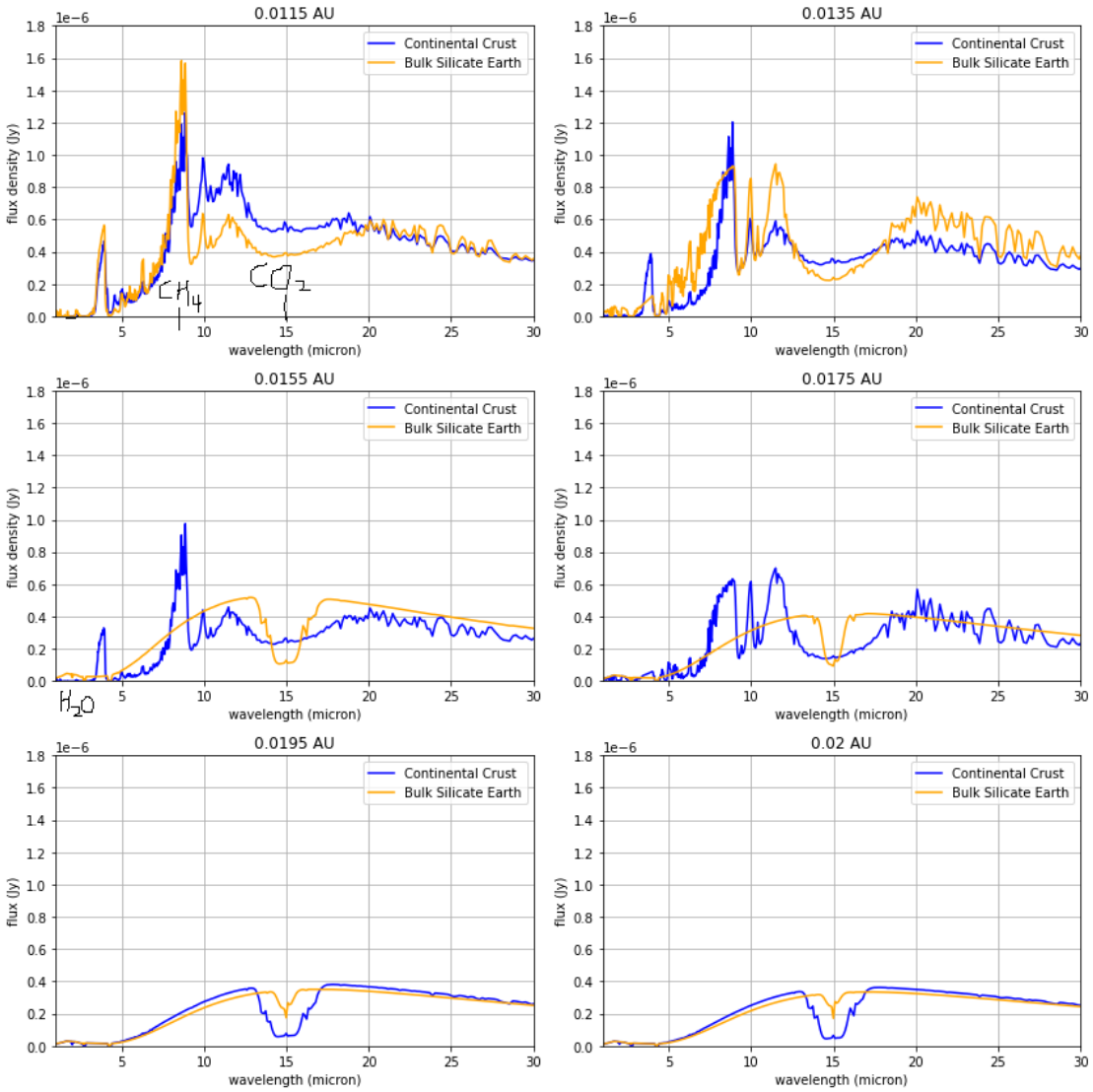

Figure 8: The emission spectra of the simulated planets using the same intervals of orbital radius as Figure 7.

,

As we see in Figure 9, the outgassed CC-atmosphere starts out very CO_2 dominated, but the CO_2 abundance drops significantly as orbital radius is increased, with the atmosphere eventually becoming more N_2 dominated. BSE-atmospheres start out with less CO_2 and eventually become N_2 dominated as well, although this happens more quickly than for CC-atmospheres. For BSE, we also see a sharp decrease in methane, occurring lower and lower in the atmosphere as the orbital radius is increased.

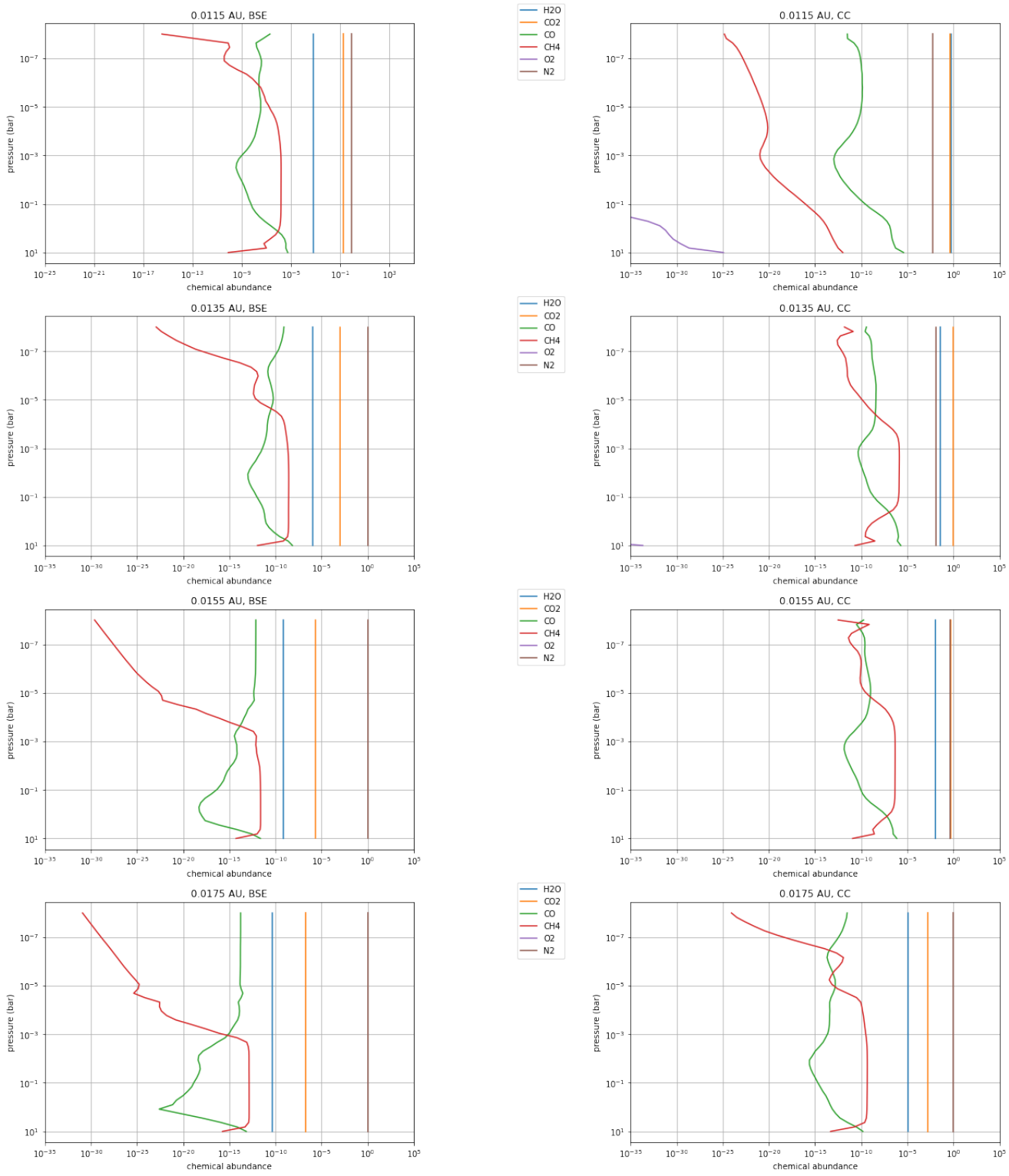

Figure 9: The abundance as a function of pressure in double logarithmic scale, evolving as orbital radius is increased. To improve readability, it was chosen to go no further than 0.0175 AU as this was enough to study the temperature order shift.

,

4.5 Night to Day Flux Ratios

In Figure 10, we plot the night to day flux ratio as a function of surface pressure. We can see that the night to day flux ratio resembles a power law correlation where the exponent is a fraction. The difference between day and night seems to decrease relatively quickly, but this slows down as pressure increases. For all planets this correlation seems to be of similar shape, although the ratios do differ in magnitude. The order of the curves seems to correspond with the order of equilibrium temperatures, as TRAPPIST-1b has the lowest equilibrium temperature of the three (Koll, 2022) and the largest night to day ratio, and LHS3844b the highest equilibrium temperature (Koll, 2022) and the smallest night to day ratio.

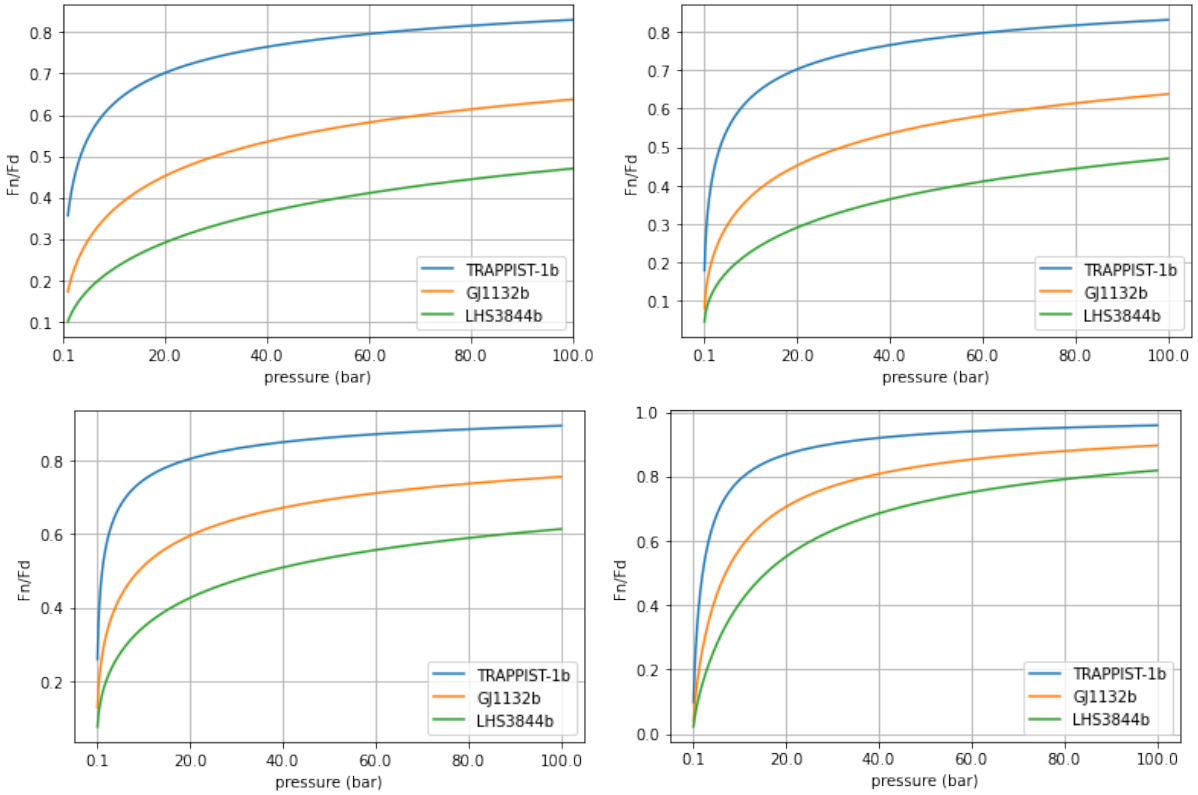

Figure 10: Night to day flux ratios plotted as a function of surface pressure varied from 0.1 to 100 bar calculated using the python function 'daynight' (see Appendix A). k and T_{eq} were taken from Koll (2022) for the planets TRAPPIST-1b, GJ1132b and LHS3844b. Top left: $\tau_{LW} = 0.1$, top right: $\tau_{LW} = 1$, bottom left: $\tau_{LW} = 5$, bottom right: $\tau_{LW} \propto P_s$. For clarity, $n/d = 0$ would mean no flux on the night side so we would have a bare rock. $n/d = 1$ would mean no difference between the day and night side.

As we vary τ_{LW}, we see that neither the order of the curves nor the basic shape changes. we do see that the night to day ratio increases with increased τ_{LW} at higher pressures for all three planets, and that the planets' curves grow more closely together, especially for $\tau_{LW} \propto p_s$, where the ratio also seems to be the largest at higher pressures for all three planets.

4.6 Emission Spectra of Day and Night Sides

In Figure 11 below, we plot emission spectra of the day and night sides as the surface pressure (and thus the night to day flux ratio) is varied four times. As we increase the night to day flux ratio, the emission spectra of the day and night sides grow to resemble each other more and more, which is what would be expected. In the next section, this figure is used as a reference to check visibility through JWST.

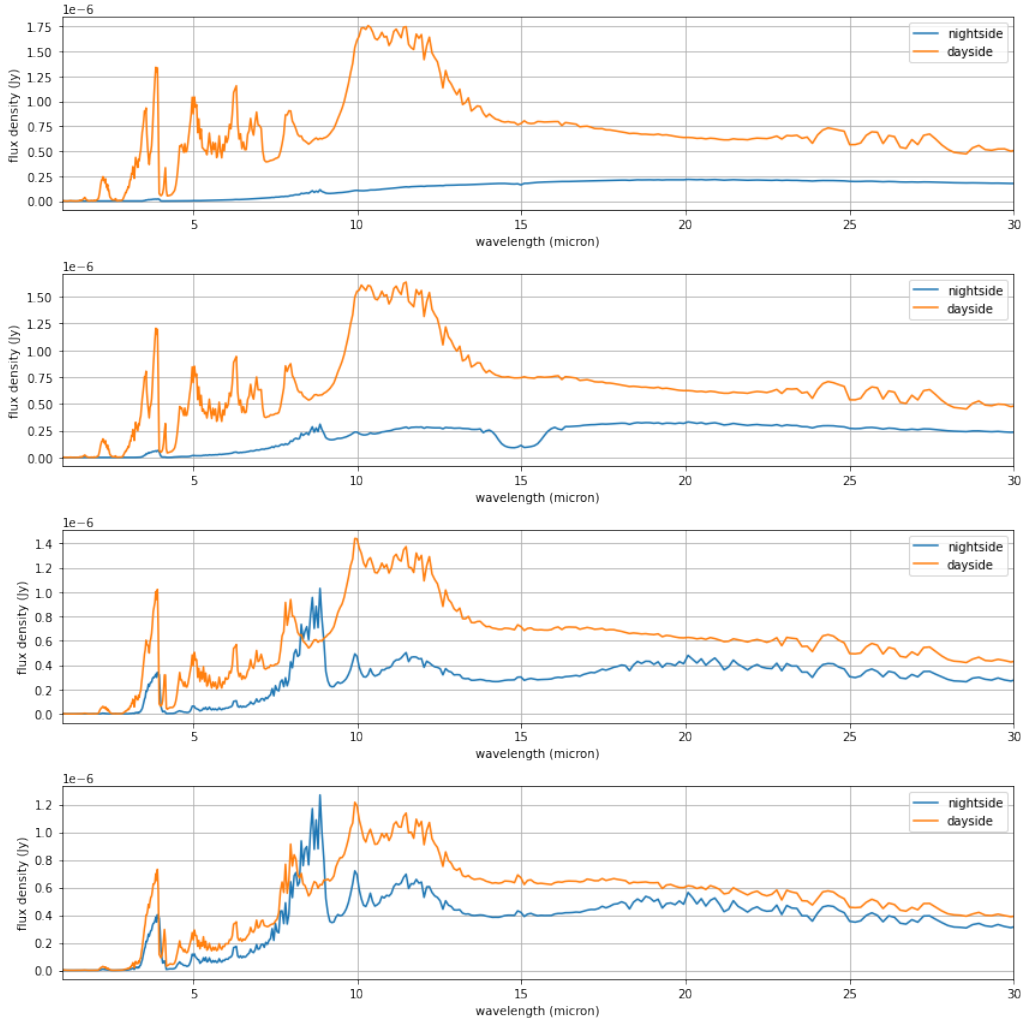

Figure 11: Emission spectra for the day and night sides calculated in ARCiS with varied surface pressures and night to day ratios calculated with the daynight function. Top: $p_s = 0.1$ bar, $n/d \approx 0.098$, second from top: $p_s = 1$ bar, $n/d \approx 0.2$, second from bottom: $p_s = 10$ bar, $n/d \approx 0.42$, bottom: $p_s = 100$ bar, $n/d \approx 0.69$.

5 Discussion

In this section, an interpretation is given of the results. First, the processes behind the temperature switch between BSE- and CC-atmospheres are discussed, as well as the sudden temperature jump that seems to appear for BSE-atmospheres as orbital radius is increased.

In the second part, a check was made for our daynight function, to see if the results match up with what would be expected from literature, as well as a discussion of why we see the aforementioned pattern of the curves drawing closer. It is also discussed whether and how this daynight function can be used to calculate the night to day flux ratio for any tidally locked rocky exoplanet orbiting an ultracool star.

Finally, JWST measurements of the day side flux of TRAPPIST-1b taken from literature are compared to our emission spectra to see if the differences in flux are visible through JWST.

5.1 The Differences Between the Various Crust Types

Before we discuss the temperature shift due to orbital radius increase, it is important to explain why there are differences in the atmospheric temperature profiles at all through the outgassing of the different crust types.

As discussed in Section 2.1, Bulk Silicate Earth is very poor in carbon containing molecules compared to the other three, which means that less carbon dioxide and methane would be outgassed. This is also confirmed in Figure 9, where it is clearly seen that BSE-atmospheres contain less of these molecules than CC-atmospheres. Continental Crust not only contains more carbon, but also more oxides, which means even more carbon dioxide can be formed through outgassing.

MORB-atmospheres are very similar to CC-atmospheres in terms of temperature behavior except for that the temperature at high pressures is higher than for CC-atmospheres. MORB is very poor in silicates and very metallic, meaning that it, like Continental Crust, contains many oxides. It has however, a higher density than Continental Crust (3.0 g/cm^3 for MORB versus 2.7 g/cm^3 for CC (Blake et al., 2008)) and therefore more carbon dioxides and other greenhouse gases can be outgassed, making the overall temperature of planets with MORB-atmospheres (especially at the surface) higher than planets with CC-atmospheres.

CI-chondrite-atmospheres seem to be the most peculiar of the four. They seem to drop in temperature rapidly as we go higher up into the atmosphere, and then rise very quickly again relative to the rest. As CI-chondrite is very rich in light elements which are easily outgassed, as well as in carbon, we have a very light atmosphere with a relative high amount of greenhouse gas. This means that CI-chondrite atmospheres trap more heat at the surface than the other three atmospheres, but this trapping of heat decreases rapidly due to density being relatively low.

5.2 The Processes Behind the Temperature Shift

As was seen in Section 4.3, a temperature shift between CC-atmospheres and BSE-atmospheres seems to occur when orbit radius is increased. From Figures 8 and 9 it is apparent that CC-atmospheres seem to contain more CO_2 than BSE-atmospheres. For BSE-atmospheres, we also seem to detect a strong decrease in the amount of CH_4 occurring lower and lower in the atmosphere as orbital radius is increased, meaning BSE-atmospheres contain overall less greenhouse gases than CC-atmospheres. This would explain why for continental crust, the surface temperature is greater than for bulk silicate earth, as more greenhouse gases would trap heat at the surface, warming up the planet.

However, what is so interesting about greenhouse gases is that by themselves, they do not heat up so much at all. They are very opaque in the infrared range, meaning they trap a lot of

thermal radiation, but they are very transparent in the optical range, meaning they do not absorb a lot of direct heat Przyborski (2009). This is why temperatures are lower as we go higher up in the atmosphere. Seeing as both the methane decrease occurs lower and lower in the atmosphere, and the smoothening of the emission spectrum occurs more quickly for BSE-atmospheres as we increase orbital radius, this explains why the temperature order shift not only occurs, but also occurs gradually.

We also see when we look at the emission spectra (Figure 8), that they both smooth out, but that for BSE-atmospheres, the smoothening of the emissions occurs much more quickly than for CC-atmospheres. When we look at a smooth radiation curve, we are looking at emission directly from the planet's surface, because the molecular abundances become quite low except for that of CO_2, meaning that very litle emission from the surface is absorbed.

The sudden jump in temperature that seems to occur for BSE-atmospheres does not seem to be a realistic phenomenon. One would not expect the temperature to fall to below 100 K and then suddenly jump to over 200 K after such a small pressure decrease. Therefore it is likely to be a limitation of the ARCiS program itself. This might be explained through the smoothening of the emission spectra discussed earlier. When the curve becomes too smooth there is little to no molecular abundance left in the atmosphere. ARCiS calculates the temperature profiles through the chemistry (Figure 3). The temperature profiles may become less accurate if there is not enough chemical abundance from the outgassing process.

5.3 The Processes Behind the Night to Day Ratio Differences

In Figure 10, we see that the shape of the night to day flux ratio versus surface pressure correlation does not change radically. We see that the night to day ratio increases when surface temperature is increased, but the rate of increase slows down gradually. It is also apparent that this slowing down of the rate of increase occurs differently for each of the three planets. As τ_{LW} is increased, the curves seem to grow more similar to one another, and the curves seem to become more sharp, with the rate of increase slowing down more rapidly. This is also what we would expect looking at Figures 13 and 14 (Appendix B), seeing as with an increase of surface pressure, the day time temperature decreases, and the night time temperature increases.

In Table 1 (see Appendix B) we see that the equilibrium temperatures and k-values of the three planets are different. TRAPPIST-1b has the lowest equilibrium temperature as well as the lowest k-value. LHS3844b seems to have the highest equilibrium temperature and k-value. The order seems to correspond to what we see in Figure 10, as TRAPPIST-1b seems to have the highest overall night to day ratio, and therefore has the lowest difference between the day- and night side flux, and therefore also between the temperatures.

The processes behind this, with regard to the equilibrium temperatures, revert to thermal heating and cooling processes. As said before, a higher equilibrium temperature directly corresponds to a higher amount of radiation the planet receives from its host star. As the planet is bombarded by radiation, it speeds up the heating rate on the planet, which in turn also causes the planet to radiate more heat outward and thus cool more efficiently, assuming that trapping of heat by greenhouse gases is equal on all three planets. This would cause a greater difference between the day and night side flux on the planet and explains partially why the rate of increase is so different for each of the three planets.

The other difference, regarding the k-value can be explained through equation 3. If we increase g, we increase the value of k, and thus increase the day side flux (equation 2), while decreasing the night side flux (equation 4), causing a greater difference in day and night side flux, and thus a smaller night to day flux ratio.

When we increase τ_{LW}, the night to day ratio increases for each of the three planets. This

is because if long wave optical thickness is increased, there is a more opaque atmosphere which allows less radiation in, cooling the day-side, while also distributing heat more evenly across the planet, warming up the night side. This causes a smaller difference between day- and night-side flux, which is what is seen in Figure 10.

If τ_{LW} is proportional to the pressure itself (depicted by the bottom right plot in Figure 10), an increase in pressure also causes an increase in optical thickness. It would therefore be expected that the night to day flux ratio increases more sharply, which is also what is seen in Figure 10 (bottom right), comparing it to the rest of the plots, where a constant optical thickness is assumed.

From Figures 13 and 14 (see Appendix B), the results are confirmed further, as we see that day-side temperatures decrease with increasing pressure, and the night-side temperatures increase with increasing pressure. We see that at lower pressures, the difference should be the highest, and at higher pressure, the difference should be the lowest.

It can therefore safely be said that the daynight calculator works within its assumptions. If equilibrium temperature, surface gravity, planet mass, atmospheric pressure and long wave optical thickness are known, it is possible to calculate the night to day flux ratio for any tidally locked rocky exoplanet orbiting an ultracool star.

5.4 Visibility of the Flux Differences with JWST

To check for visibility of the flux differences with JWST, several factors need to be taken into account. First of all it is important to assess whether JWST can measure flux density in a range where the differences are noticeable. In our case, this would mean that JWST has to be able to measure flux densities of the order 10^{-6} Jy. Furthermore, it is important to assess in which range of wavelengths it can make measurements.

From Figure 12 (Greene et al., 2023), it is seen that the range of wavelengths the MIRI element of JWST is able to measure is the 10-20 μm range, which puts it in a good position as this is where the most prominent differences in the emission spectra are visible for TRAPPIST-1b (see Figure 11). Furthermore, it is seen that the flux density measurements by the MIRI element of JWST are of the order 10^{-6} Jy, which is consistent with our results, meaning that a difference in flux between the day- and night-sides of the planet should be visible with the MIRI element of JWST.

Whether or not the flux differences are visible is also dependent on whether both faces of the planet are observable. This would depend on the method of observation. If the transit method is used, we can obtain very clear flux densities of the night side, as that side approximately faces the telescope during transit. Its day side can also be measured using its eclipse. Direct imaging could also be used to measure flux directly. If the transit method or direct imaging cannot be used, observing day and night side differences is impossible.

TRAPPIST-1b is a planet observed through the transit method, and as such, both its day- and night- side flux should be observable. As it was shown that JWST can measure in the correct range for both the flux density and the wavelength, it is concluded that JWST is very well capable of detecting the flux differences, and therefore measure temperature differences between the day- and night sides of tidally locked rocky exoplanets orbiting ultracool stars.

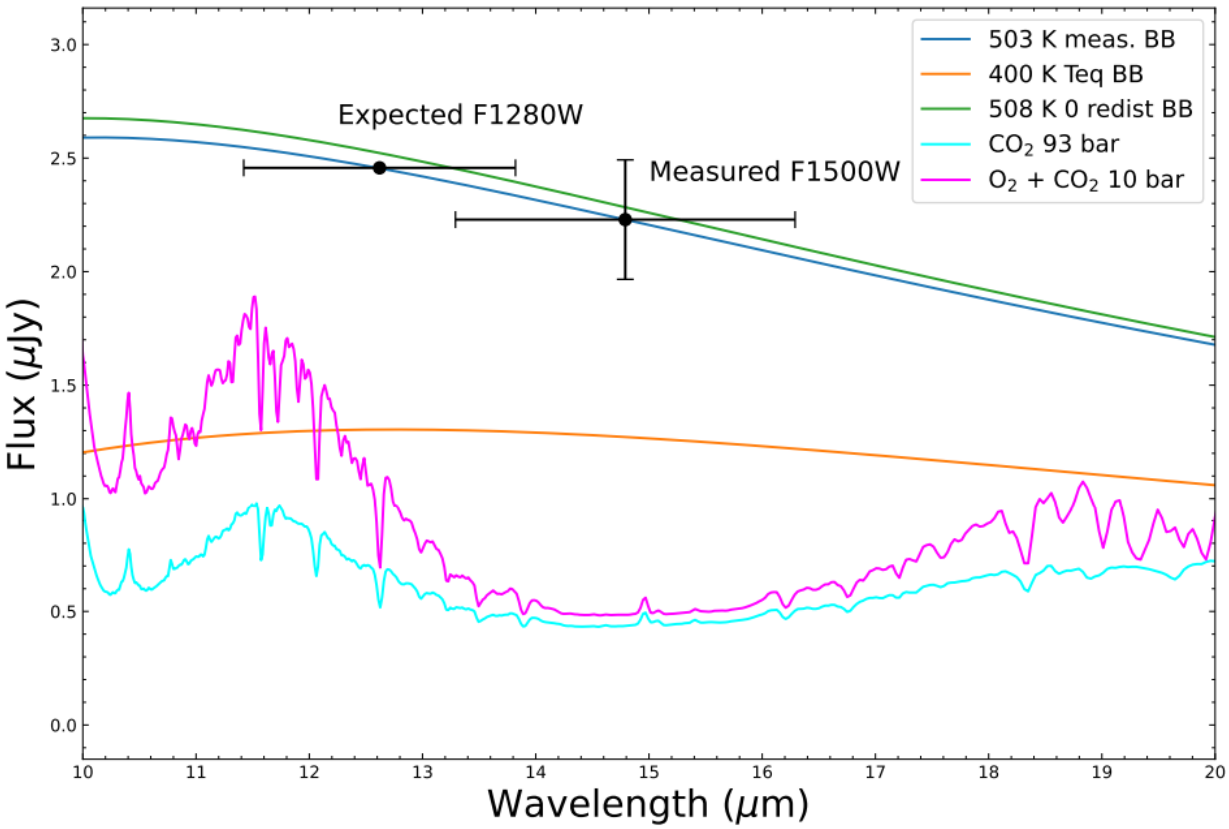

Figure 12: A spectrum of the day-side of TRAPPIST-1b observed with the MIRI element of JWST. The measurements were compared to a simulation assuming a blackbody (the smooth curves). The light blue and pink curves represent the direct measurements, while the smooth curves reperesent the blackbody simulations. See Greene et al. (2023) for more details on how this was obtained.

6 Conclusion

In this research, the temperature profiles of exoplanet atmospheres were studied using an outgassing simulation program called ARCiS. Four generic crust types were studied by comparing their temperature structures. Other variables were varied as well, such as planet mass, radius, albedo and orbital radius. Furthermore, differences in temperature on the day- and night sides were studied by calculating the night to day flux ratio and looking at its dependence on pressure, using three different planets with different equilibrium temperatures. Visibility with JWST was also studied by plotting emission spectra of the day and night sides of TRAPPIST-1b, assuming a CC-atmosphere and and comparing these results to measurements from literature.

For the temperature behavior we see that different crust types result in atmospheres with different temperature structures. This is because of several factors, such as the amount of carbon and oxidates that are in the crust, as well as the evaporation temperatures of the chemicals of which the crust is composed. An increase in the outgassing of greenhouse gases would result in higher surface temperatures, but lower temperatures in the upper atmosphere, as greenhouse gases are very transparent to optical wavelengths, but very opaque to infrared wavelengths.

A switch in temperatures occurs between BSE-atmospheres and CC-atmospheres as orbital radius is increased. This switch in temperatures is also caused by the amount of greenhouse gases, as it is apparent from Figures 8 and 9 that BSE-atmospheres contain less greenhouse gases such as CO_2 and methane than CC-atmospheres. BSE-atmospheres even undergo a severe drop in methane higher up in the atmosphere, which seems to occur lower and lower in the atmosphere as orbital radius is increased. CC-atmospheres do not undergo this change as much. This phenomenon can thus be explained by the same properties of greenhouse gases, as they trap heat at the surface by blocking infrared light, but they do not absorb a lot of optical light, so higher up in the atmosphere, temperatures are lower.

For BSE-atmospheres, an unexpected temperature spike was observed, which seems to form as orbital radius is increased. This spike is caused by ARCiS having trouble computing temperatures for atmospheres containing too little abundance of diverse molecules, as these emissions seem to come directly from the planet's surface. For future research, it may be useful to improve ARCiS to compute more accurate temperature profiles for transparent atmospheres.

For the night to day flux ratios, we see that as we increase pressure, the night to day flux ratio increases, but for higher pressures, the rate of this increase slows down. For the three different planets, we see that the correlation becomes different, with planets with a higher equilibrium temperature and k-value, having an overall lower night to day flux ratio and thus more difference between their day and night side. The overall shape of the correlation does not change radically.

As all three planets are assumed to have the same surface pressure in this simulation, this difference in correlation can be explained by the processes behind heating and cooling rates. If equilibrium temperature is increased, and all of the planets' internal properties are not altered, the amount of radiation from the host star is increased, meaning that the planet is heated up more quickly on the day side, but the night side does not receive this stellar radiation, meaning it does not warm up as much. This causes a greater temperature difference between the day- and night sides.

The k-value, which is proportional to gravitational acceleration, would cause a difference in night to day flux ratios because of planet gravity. As we increase gravitational force, this increases the k-value, in turn increasing the day side flux, and decreasing the night side flux further. This causes an even greater difference between the day and night sides.

When the value of τ_{LW} is increased, we see that the night to day flux ratio increases for all three planets. This is especially apparent when τ_{LW} is directly proportional to the surface pressure. If we increase the optical thickness, less light is allowed in, but heat is distributed more

evenly across the planet, causing the day side to cool down and the night side to warm up. This decreases the difference between the day and night sides.

Overall, no peculiarities are visible in the results of the night to day flux ratio versus pressure, and the daynight calculator can in principle be used to determine this ratio for any tidally locked rocky exoplanet orbiting an ultracool star. In future research, it might be useful to take into account non-tidally locked planets, or other types of planets like gas giants.

Lastly, the comparison of the emission spectra of the day and night sides to those of Greene et al. (2023) shows that the MIRI-element of JWST can not only observe in the right flux range of 10^{-6} Jy, but it also observes a wavelength range which is ideal for observing difference in day and night sides, as differences are most visible between 10 and 20 μm. It is therefore concluded that JWST should be able to see differences in infrared flux between the day and night sides.

For future research, it may be useful to use different planet base models than TRAPPIST-1b and use different crust types than CC, to see if the differences between the two sides change. It could very well be that for planets with different atmospheres, the range of 10 to 20 μm is not so ideal, and so it is important to narrow this down.

All in all, the atmospheres of rocky exoplanets are very dynamic and have many properties that intermingle with one another. This research only covers a tiny fraction of what exoplanets have to offer in terms of knowledge. In the future we may want to expand to different types of exoplanets like gas giants, or narrow it down to more specific types of rocky exoplanets, like super-Earths. We may also want to expand to non-tidally locked planets or planets orbiting different types of stars. Other natural phenomena, like magnetic fields, would also have an effect on atmosphere formation and would also be important to take into account.

Appendix A: Code

See below for the python code which details a function which calculates the night to day flux ratio for any tidally locked rocky exoplanet orbiting an ultracool red dwarf star.

```
def daynight(k, tlw, Teq, ps):
    """returns the ratio of night-side flux over day-side flux
    for a rocky exoplanet. the input value k is a collection of
    planetary parameters, tlw is the planet's gray optical thickness,
    Teq is the equilibrium temperature and ps is the
    planet's surface pressure (bar)."""

    sigma = 5.6704 * 10**(-5) #cm^2 g s^-2 K^-1 stefan boltzmann constant in cgs units

    # night side flux

    Fn_num = 1/k * ((ps * tlw)/Teq**4)**(1/3) * 1**(-2/3) * 600**(4/3) # numerator
    Fn = (Fn_num/(1 + Fn_num)) * sigma * Teq**4 # final flux

    # day side flux

    Fd_num = tlw**(1/3) * (ps/1)**(2/3) * (Teq/600)**(-4/3)
    Fd = ((8/3) - (5/3) * Fd_num/(k + Fd_num)) * sigma * Teq**4

    ratio = Fn/Fd

    return ratio
```

Appendix B: Figures and Tables

	Radius ($R_\oplus$)	Period (days)	Surf. Gravity (m s^{-2})	T_{eq} [a] (K)
TRAPPIST-1b	1.12	1.51	7.95	391
GJ1132b	1.16	1.63	11.8	578
LHS3844b	1.32	0.46	12.9[b]	805

Table 1: properties of the three planets used in the calculation of the night to day ratio versus surface pressure plots (Koll, 2022).

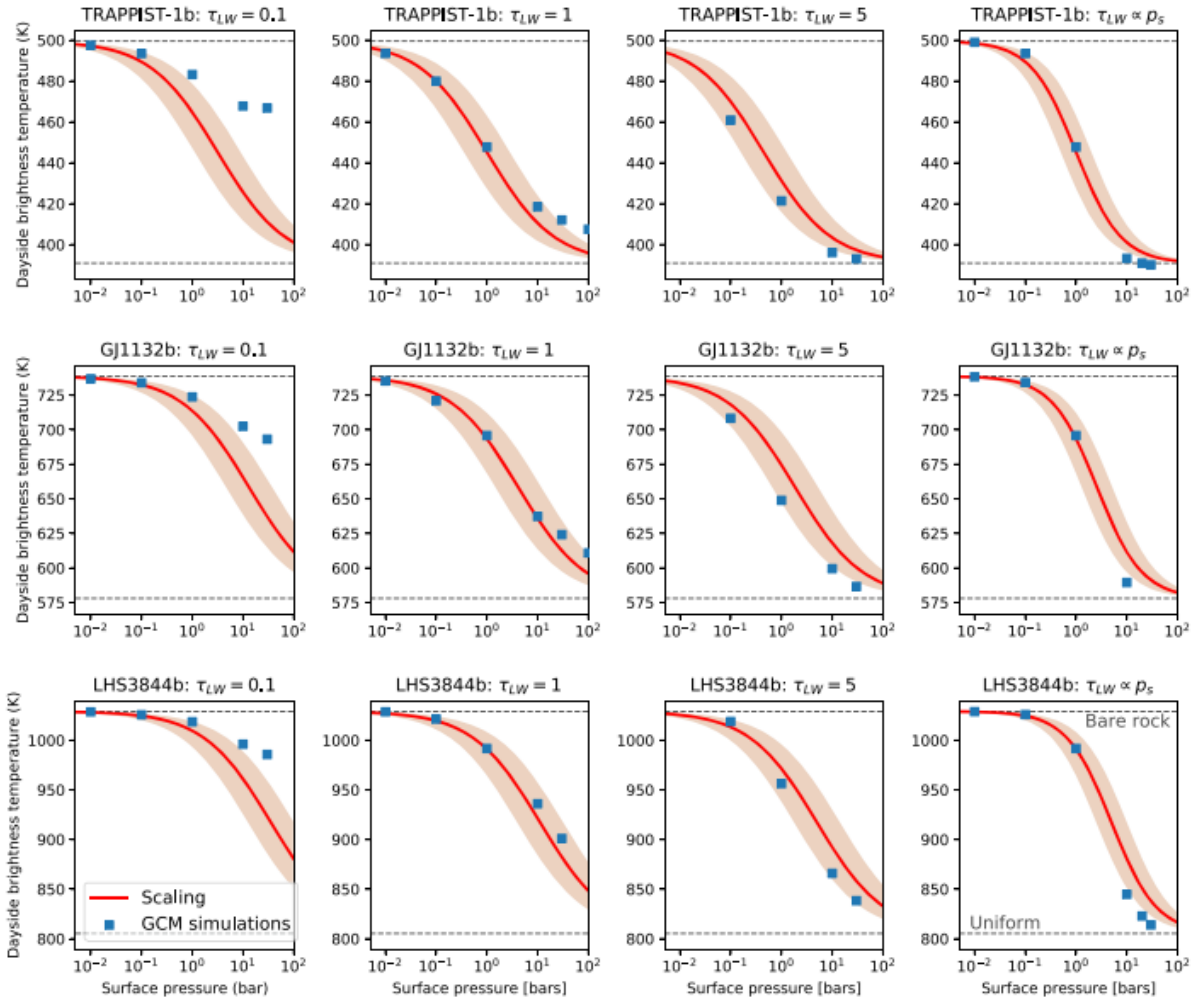

Figure 13: A figure taken from Koll (2022) depicting a simulation of the effect on the day-side temperature of increasing surface pressure, for several values of τ_{LW}.

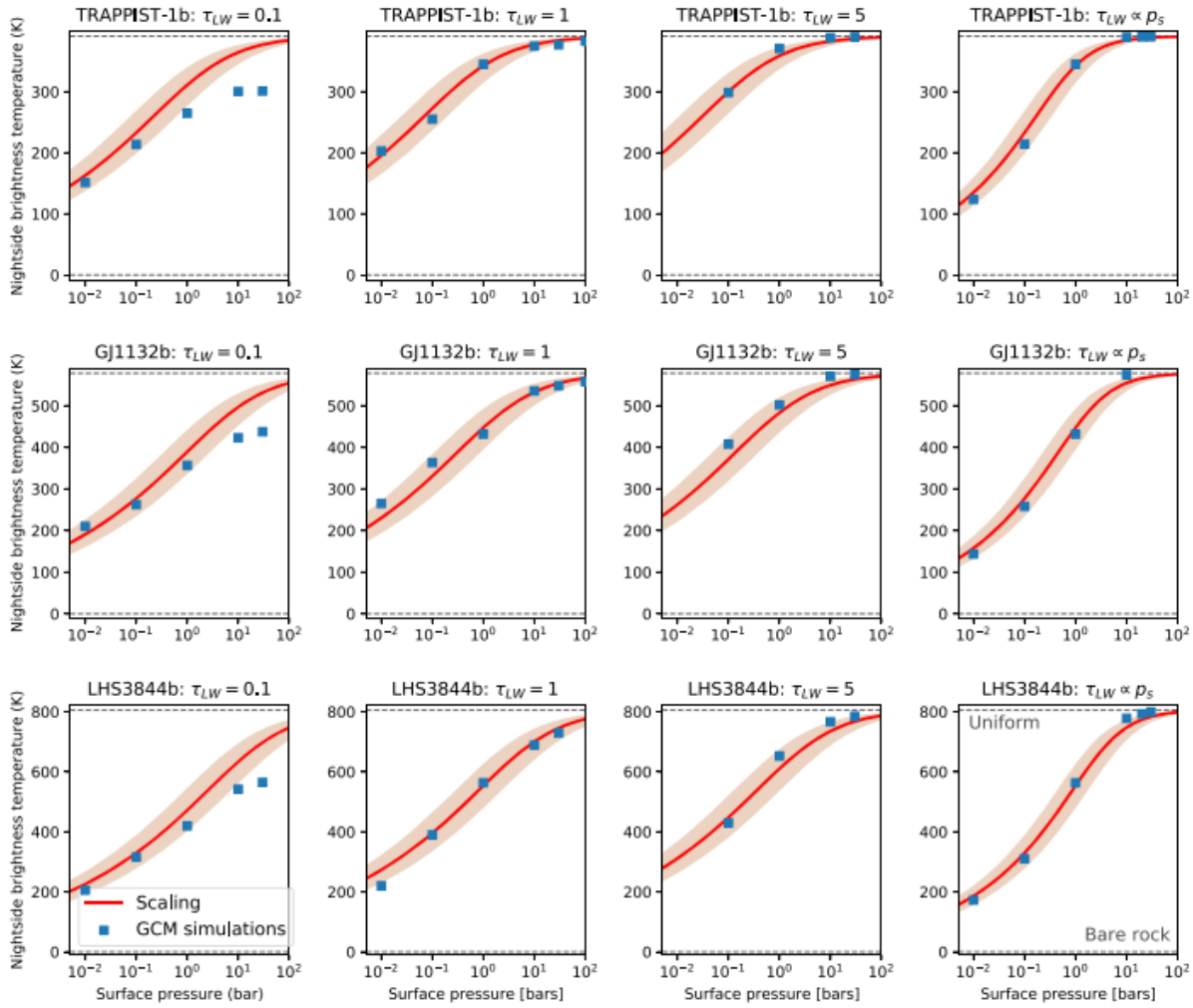

Figure 14: A figure taken from Koll (2022) depicting a simulation of the effect on the night-side temperature of increasing surface pressure, for several values of τ_{LW}.

	BSE 1	BSE12 1(*)	BSE15 1 (*)	CC 2	MORB 3	CI 4
H	0.006	1.198	1.457	0.045	0.023	1.992
C	0.006	0.0054	0.005	0.199	0.019	3.520
N	8.8E-05	7.9E-05	7.7E-05	0.006	5.5E-05	0.298
O	44.42	49.280	50.320	47.20	44.5	46.420
F	0.002	0.0018	0.0017	0.053	0.017	0.0059
Na	0.29	0.260	0.253	2.36	2.012	0.505
Mg	22.01	19.69	19.180	2.20	4.735	9.790
Al	2.12	1.897	1.847	7.96	8.199	0.860
Si	21.61	19.33	18.830	28.80	23.62	10.820
P	0.008	0.0072	0.0070	0.076	0.057	0.098
S	0.027	0.024	0.024	0.070	0.110	5.411
Cl	0.004	0.0036	0.0035	0.047	0.014	0.071
K	0.02	0.018	0.017	2.14	0.152	0.055
Ca	2.46	2.201	2.143	3.85	8.239	0.933
Ti	0.12	0.107	0.105	0.401	0.851	0.046
Cr	0.29	0.260	0.253	0.013	0.033	0.268
Mn	0.11	0.098	0.096	0.072	0.132	0.195
Fe	6.27	5.610	5.463	4.32	7.278	18.710
sum	99.77	99.99	100.00	99.81	99.99	100.00

Table 2: atomic abundances of six different crust types, including BSE, CC, MORB and CI-chondrite (Herbort et al., 2021).

Appendix C: An Example of an ARCiS Input File

```
Na=0.225853946
SiO=0.173465965
H2O=0.101574898
K=0.091236907
O2=0.059899219
OH=0.041215460
O=0.023121555
SiO2=0.016011261
H2=0.015506486
H=0.014833490
CO=0.002822079
SO2=0.002678777
N2=0.000055185
CO2=0.002363912
CH4=1.8d-6
H2S=1d-4
PH3=1d-4
TiO=1d-4
VO=1d-4

Rp=0.08d0
Mp=0.00256d0
Pp=0.01d0
TeffP=10d0

Tstar=5777
Rstar=1d0
distance=14.9

Dplanet=0.7d0

chemistry=.true.
condensates=.false.
simplerainout=.false.

elementfile='/Users/users/ferdinand/ARCiS/Data/atom_abun/abund_CC.dat'

secondary_atmosphere=.true.

pmin=1d-8
pmax=1d1
Pp=1d1

nr=50

lmin=0.1d0
```

```
lmax=50.0d0

specres=150

cia=.true.
cia1:file="/Users/users/ferdinand/ARCiS/Data/CIA/CO2-CO2_combined.cia"

computeT=.true.

scattering=.true.
scattstar=.true.

maxiter=30

emisspec=.true.

par_tprofile=.true.

run3D=.true.
night2day=1d0
```

References

Blake, S., Burton, K., Harris, N., Parkinson, I., Rogers, N., and Widdowson, M. (2008). *An introduction to our dynamic planet*. Cambridge Univ. Press [u.a.], 1. publ edition.

Brady, M. T., Bean, J. L., Seifahrt, A., Kasper, D. L., Luque, R., Reiners, A., Benneke, B., Stefansson, G., and Stürmer, J. (2023). Measuring the obliquities of the trappist-1 planets with maroon-x. 165:129–129.

Brennan, P. (2019a). 5 ways to find a planet | explore – exoplanet exploration: Planets beyond our solar system.

Brennan, P. (2019b). How many exoplanets are there? – exoplanet exploration: Planets beyond our solar system.

Crane, L. (2023). Jwst telescope finds trappist-1b may have no atmosphere. 257:13–13.

Del Genio, A. D., Kiang, N. Y., Way, M. J., Amundsen, D. S., Sohl, L. E., Fujii, Y., Chandler, M., Aleinov, I., Colose, C. M., Guzewich, S. D., and Kelley, M. (2019). Albedos, equilibrium temperatures, and surface temperatures of habitable planets. *The Astrophysical Journal*, 884:75.

Dobos, V., Barr, A. C., and Kiss, L. L. (2019). Tidal heating and the habitability of the trappist-1 exoplanets. *Astronomy Astrophysics*, 624:A2.

Gillon, M., Jehin, E., Lederer, S. M., Delrez, L., de Wit, J., Burdanov, A., Van Grootel, V., Burgasser, A. J., Triaud, A. H. M. J., Opitom, C., Demory, B.-O., Sahu, D. K., Bardalez Gagliuffi, D., Magain, P., and Queloz, D. (2016). Temperate earth-sized planets transiting a nearby ultracool dwarf star. *Nature*, 533:221–224.

Greene, T. P., Bell, T. J., Ducrot, E., Dyrek, A., Lagage, P.-O., and Fortney, J. J. (2023). Thermal emission from the earth-sized exoplanet trappist-1 b using jwst. *Nature*.

Grimm, S. L., Demory, B.-O., Gillon, M., Dorn, C., Agol, E., Burdanov, A., Delrez, L., Sestovic, M., Triaud, A. H. M. J., Turbet, M., Bolmont, , Caldas, A., Wit, J. d., Jehin, E., Leconte, J., Raymond, S. N., Grootel, V. V., Burgasser, A. J., Carey, S., Fabrycky, D., Heng, K., Hernandez, D. M., Ingalls, J. G., Lederer, S., Selsis, F., and Queloz, D. (2018). The nature of the trappist-1 exoplanets. *Astronomy Astrophysics*, 613:A68.

Herbort, O., Woitke, P., Helling, C., and Zerkle, A. L. (2021). The atmospheres of rocky exoplanets. ii. influence of surface composition on the diversity of cloud condensates. *Astronomy Astrophysics*.

Kite, E. S. and Barnett, M. N. (2020). Exoplanet secondary atmosphere loss and revival. *Proceedings of the National Academy of Sciences*, 117:18264–18271.

Koll, D. D. B. (2022). A scaling for atmospheric heat redistribution on tidally locked rocky planets. *The Astrophysical Journal*, 924:134.

Min, M., Hovenier, J. W., and de Koter, A. (2005). Modeling optical properties of cosmic dust grains using a distribution of hollow spheres. *Astronomy and Astrophysics*, 432:909–920.

Min, M., Ormel, C. W., Chubb, K., Helling, C., and Kawashima, Y. (2020). The arcis framework for exoplanet atmospheres. *Astronomy Astrophysics*, 642:A28.

NASA (1968). Venus air pressure.

Noack, L., Rivoldini, A., and Van Hoolst, T. (2017). Volcanism and outgassing of stagnant-lid planets: Implications for the habitable zone. *Physics of the Earth and Planetary Interiors*, 269:40–57.

Pater, I. D. and Lissauer, J. J. (2015). Planetary sciences.

Przyborski, P. (2009). Climate and earth's energy budget.

Woitke, P., Helling, C., Hunter, G. H., Millard, J. D., Turner, G. W., Worters, M., Blecic, J., and Stock, J. W. (2018). Equilibrium chemistry down to 100 k. *Astronomy and Astrophysics*, 614:A1–A1.